

~~Adiabatically~~ Quasi-Objective Eddy Visualization from Sparse Drifter Data

Alex P. Encinas Bartos, Nikolas Aksamit and George Haller*

Institute for Mechanical Systems
ETH Zürich

April 12, 2022

Abstract

We employ a recently developed single-trajectory Lagrangian diagnostic tool, the trajectory rotation average ($\overline{\text{TRA}}$), to visualize oceanic vortices (or eddies) from sparse drifter data. We apply the $\overline{\text{TRA}}$ to two drifter datasets that cover various oceanographic scales: the Grand LAgrangian Deployment (GLAD) and the Global Drifter Program (GDP). Based on the $\overline{\text{TRA}}$, we develop a general algorithm that extracts approximate eddy boundaries. We find that the $\overline{\text{TRA}}$ computed from sparse drifter data outperforms existing single-trajectory based eddy detection mechanisms.

Summary

Meso and submesoscales vortices (or eddies) can trap and transport material over large distances, thereby playing a crucial role in the dynamics of our ecosystem. In order to expand our understanding of the transport of marine tracers, we need to accurately and reliably track the evolution of vortical flow structures. Drifter trajectories represent a valuable but sparse source of information for this purpose. We employ a single-trajectory Lagrangian diagnostic tool, that approximates the local material rotation in the flow. Our findings on two distinct datasets suggest that the selected rotational flow diagnostic accurately highlights vortical flow structures from sparse drifter data.

1 Introduction

Oceanic vortices (or eddies) are highly energetic coherent flow structures which can transport material over large distances. Studying the dynamics of eddies is key to understanding the dispersion of marine tracers, such as biological nutrients and pollution particles [62, 15, 4, 41, 2]. Lagrangian eddies, generally referred to as elliptic Lagrangian coherent structures (LCS) in dynamical systems theory [22], are material objects which can trap and transport floating particles over large distances in the ocean. Eddy sizes range from a few kilometers (submesoscale) to hundreds of kilometers (mesoscale). Mesoscale eddies have predominantly been inferred from the sea-surface-height (SSH) profile derived from satellite altimetry data [11, 14, 29, 1]. There is, however, increasing evidence that submesoscale currents on the order of a few kilometers influence the marine ecosystem at least as strongly as mesoscale eddies, especially along coastlines and oceanic fronts [39, 28]. Despite this, submesoscale eddies are rarely studied in detail as their trace in the SSH field is very weak. Compared to the SSH field, which only captures the geostrophic velocity component of the ocean, drifters closely follow ocean currents thereby accurately resolving small scale features [35]. As opposed to satellite-based altimetry data, surface drifter observations provide direct and reliable information about the local ocean surface velocity field at very high temporal resolutions. Ocean drifters are, however, sparsely distributed in space, rendering most Lagrangian coherent structure (LCS) diagnostics inapplicable to their trajectories. Indeed, most mathematically justifiable algorithms for the detection of vortical Lagrangian coherent structures

*Email:georgehaller@ethz.ch

(elliptic LCSs) require differentiation with respect to initial conditions [22], which is unfeasible for sparse drifter data.

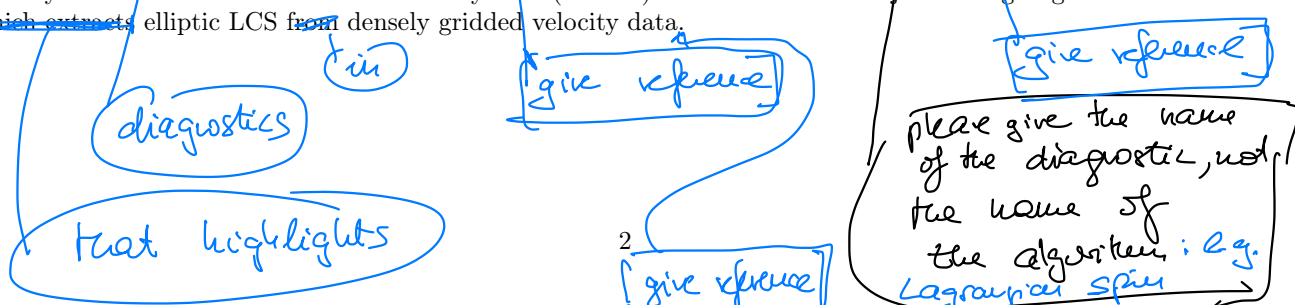
Alternatively, elliptic LCSs can be viewed as a coherently evolving set of material trajectories in space. Hence, a wide range of clustering methods for extracting elliptic LCSs have been proposed (see [21] for a review). These objective methods fundamentally distinguish themselves depending on the specific clustering algorithm and on the employed distance metric. Common algorithms include fuzzy clustering [16], spectral graph methods [20, 57] and density based clustering methods [42]. However, their results strongly rely on user defined input parameters, such as specifying the number of clusters, and hence the number of elliptic LCSs in the domain. This limitation becomes even more concerning in a sparse drifter setting where the number of eddies is a priori unknown.

Consequently, to extract elliptic LCS from drifter data, one is forced to rely on features of a single trajectory, such as trajectory length, velocity, acceleration and curvature. These features, however, are all inherently non-objective (frame-dependent) quantities whereas LCS, as material objects, are ~~independent~~^{frame, i.e., indifferent to} of the coordinate frame [22]. Therefore, common single-trajectory methods, such as the absolute dispersion [48], trajectory length [36, 37], Lagrangian spin [56], maximal trajectory extent [43], trajectory complexity [55] and wavelet ridge analysis [30], are ~~fundamentally~~ limited in capturing elliptic LCSs as they are non-objective and lack physical connection to material deformation in the fluid. Accordingly, while most of these methods were originally introduced to visualize LCSs from truly sparse trajectories, their application to drifter data has remained rare. Notable exceptions include the fully automated looper detection algorithms based on the Lagrangian spin [63, 18, 13, 35]; and the wavelet ridge regression [32]. Both methods seek to extract oscillatory motions from a time-series and lead to comparable results. The methodology employed by [63, 18, 13, 35] is an aggregate measure of rotation within a time-series of the Lagrangian spin, whereas [32] quantifies the instantaneous oscillatory motion of the velocity using signal processing techniques. Loosely speaking, elliptic LCSs are hereby visualized exclusively through looping (or oscillatory) trajectory segments.

In order to distinguish looping from non-looping trajectory segments, a user-defined threshold is inevitably required. In a practical setting, however, differentiating between looping and non-looping trajectories proves to be challenging and hence finding an appropriate parameter is far from trivial. A common approach is to manually tune the threshold value based on a subset of trajectories. Although the above mentioned procedure provides a natural and intuitive way to characterize elliptic LCSs, a considerable amount of information is lost when discarding non-looping trajectory segments. Instead, it would be ~~more appropriate~~ to retain all trajectory information and associate to each ~~and every~~ trajectory a Lagrangian diagnostic related to material rotation in the flow. The rotational diagnostic is then to be plotted over the evolving trajectory positions. This approach would provide a qualitative overview of individual vortical flow structures, without relying on any chosen threshold.

None of the aforementioned single trajectory methods, however, are suited as scalar Lagrangian diagnostic quantities for eddy visualization purposes as they are not related to underlying material deformation. Hence, these methods remain primarily statistical tools rather than detection tools for individual material structures from truly sparse data.

Here we propose to fill this gap by capitalizing on recent theoretical work by [25] on adiabatically quasi-objective single-trajectory diagnostics. Adiabatically quasi-objective quantities are close approximations of objective quantities in qualifying frames defined by computable criteria, which are expected to hold in geophysical flows. We show that the adiabatically quasi-objective trajectory rotation average (TRA) successfully identifies elliptic LCSs (material eddies) at meso-and submesoscales from sparse drifter trajectory data. We additionally compare the vortical flow features extracted from the drifter-based TRA computation with those obtained from other commonly used Lagrangian single trajectory metrics such as the trajectory length and automated looper detection algorithm. We further validate the extracted features with respect to Lagrangian averaged vorticity deviation (LAVD) computed from geostrophic ocean velocity fields derived from satellite altimetry data (AVISO). The LAVD is an objective Lagrangian rotation metric which extracts elliptic LCS from densely gridded velocity data.



2 Data

2.1 Satellite altimetry ocean-surface current product (AVISO)

The two-dimensional, satellite-altimetry-derived ocean-surface current product (AVISO) has been the focus of several coherent structure studies [46] [45] [4]. The geostrophic velocity $\mathbf{v}_g(\mathbf{x}, t)$ of ocean currents is derived from the sea-surface height η as

$$\mathbf{v}_g(\mathbf{x}, t) = \frac{g}{f} \begin{pmatrix} 0 & -1 \\ 1 & 0 \end{pmatrix} \nabla \eta \quad (1)$$

where g is the constant of gravity and f is the Coriolis parameter. A global daily-gridded version of the sea-surface height profile is freely available from the Copernicus Marine Environment Monitoring Service.

2.2 Drifter datasets

In contrast to satellite-based altimetry, surface drifter observations provide direct estimates of the local surface velocity field. In order to illustrate the range of applications of the adiabatically quasi-objective single-trajectory rotation measure introduced in [25], we focus on two drifter datasets: the Grand LAgrangian Deployment (GLAD) and the Global Drifter Program (GDP).

2.2.1 Grand LAgrangian Deployment (GLAD)

We consider the Coastal Dynamics Experiment (CODE) drifters [12], released during the Grand LAgrangian Deployment (GLAD) [45] [47] [38]. In order to study relative dispersion statistics, around 300 drifters were deployed on the 20th – 31th of July 2012 in the northern Gulf of Mexico, sampling various submesoscale features over several weeks. The positions of the drifters were reported every 15 minutes from which we estimate their velocities via finite differencing. In order to highlight important circulation features, we focus on GLAD-drifters active from the 10th to the 17th of August, restricting the domain of interest to

$$\{(x, y) \in [89.5^\circ\text{W}, 86^\circ\text{W}] \times [26^\circ\text{N}, 29^\circ\text{N}], \quad t \in [222\text{doy}, 229\text{doy}]\}. \quad (2)$$

where doy is a shorthand for ...

2.2.2 Global Drifter Program (GDP)

Additionally, we consider the Global Drifter Program (GDP) dataset, which contains more than 20,000 drifters released over the past 40 years. At least 1,000 of those drifters are now simultaneously active worldwide [34]. These drifters report their positions every 6 hours. We specifically focus on a subset of drifters active from the 4th September 2006 to the 4th October 2006 in the Gulf Stream, i.e., in the domain

$$\{(x, y) \in [72.5^\circ\text{W}, 65^\circ\text{W}] \times [32.5^\circ\text{N}, 40^\circ\text{N}], \quad t \in [246\text{doy}, 276\text{doy}]\}. \quad (3)$$

2.2.3 Drifter data preprocessing

As highlighted by [17] [5] and [52], inertial oscillations have little effect on the overall motion of nearby inertial particles as they periodically return to their starting position after one inertial period. The anticyclonic looping arising from inertial oscillations, however, ~~clearly~~ impacts the velocity profile without actually influencing separation between nearby particles. In order to remove this unwanted effect from our analysis, we apply a 6th-order low-pass Butterworth filter to the drifter trajectories with a cut-off period $T_{cut} = 1.5T_{inertial}$, as suggested by [13] [5] [35]. Here, the inertial period is

$$T_{inertial} = \frac{2\pi}{2\omega \sin(y)}, \quad (4)$$

where y is the latitudinal position of the drifter and $\omega = 7.27 * 10^{-5} \frac{\text{rad}}{\text{s}}$ is the rotation rate of the Earth.

At mid-latitudes, inertial oscillations have time-scales of 1-2 days, whereas the dominant period of submesoscale and mesoscale eddy motion is above 5 days [38]. The characteristic time of submesoscale and mesoscale features thus greatly exceeds the inertial period. Hence, the anticyclonic looping arising from high-frequency diurnal inertial oscillations does not influence the relative dispersion of drifters in the submesoscale and mesoscale regime [5].

3 Methods

The drifter trajectories $\mathbf{x}(t)$ are governed by the differential equation

$$\dot{\mathbf{x}}(t) = \mathbf{v}(\mathbf{x}, t), \quad \mathbf{x}(t) \in U \subset \mathbb{R}^2, \quad t \in [t_0, t_N], \quad \mathbf{x}(t_0) = \mathbf{x}_0. \quad (5)$$

Here \mathbf{x} is a position variable, t is a time variable and $\mathbf{v}(\mathbf{x}(t), t)$ is the underlying true surface ocean velocity field captured by the drifter data. Open-ocean mesoscale features are fairly accurately captured by satellite altimetry data [8]. However, in coastal areas, the velocity of the drifters $\mathbf{v}(\mathbf{x}, t)$ generally differs from the geostrophic velocity component $\mathbf{v}_g(\mathbf{x}, t)$ computed from AVISO due to coastal influences and windage [3]. Hence, it has to be expected that features derived from drifter trajectories generally differ from those obtained from ocean geostrophic velocities, especially in coastal areas.

3.1 Trajectory rotation average

As already noted in the Introduction, LCSs of the velocity field are material sets and hence their existence and location are objective, i.e., indifferent to the observer. All traditionally analyzed features of trajectory data (such as length, curvature, velocity, acceleration and looping) are, in contrast, observer-dependent and hence do not allow for a self-consistent identification of LCSs. To this end, [25, 26] developed several quasi-objective diagnostic tools for single trajectories that do approximate objective features of trajectories in frames verifying certain conditions. Inspired by the slowly varying nature of geophysical flow datasets, we restrict our discussion to a family of frames which are related to each other via slowly varying (\sim -adiabatic) Euclidean coordinate transformations

$$\mathbf{x} = \mathbf{Q}(t)\mathbf{y} + \mathbf{b}(t), \quad |\dot{\mathbf{Q}}|, |\ddot{\mathbf{Q}}|, |\dot{\mathbf{b}}|, |\ddot{\mathbf{b}}| \ll 1. \quad (6)$$

Under such slowly varying frame changes, the velocity $\tilde{\mathbf{v}}$ transforms nearly as an objective vector:

$$\tilde{\mathbf{v}} = \mathbf{Q}^T(\mathbf{v} - \dot{\mathbf{Q}}^T\mathbf{y} - \dot{\mathbf{b}}) \sim \mathbf{Q}^T\mathbf{v}, \quad (7)$$

where \mathbf{v} and $\tilde{\mathbf{v}}$ respectively denote the velocity in the original and in the slowly varying frame. We refer to a quantity as adiabatically quasi-objective if in all frames related to each other via eq. 6, the quantity approximates the same objective quantity in frames satisfying a set of conditions.

We apply one of these single-trajectory rotation diagnostics here, for the first time, to actual sparse drifter data. Similarly to [25], we consider discretized drifter trajectories $\{\mathbf{x}(t_i)\}_{i=0}^N$ cf eq.(5). As shown in [25, 26], the trajectory rotation average

$$\overline{\text{TRA}}_{t_0}^{t_N}(\mathbf{x}_0) = \frac{1}{t_N - t_0} \sum_{i=0}^{N-1} \cos^{-1} \frac{\langle \dot{\mathbf{x}}(t_i), \dot{\mathbf{x}}(t_{i+1}) \rangle}{|\dot{\mathbf{x}}(t_i)| |\dot{\mathbf{x}}(t_{i+1})|} \quad (8)$$

measures the time-averaged angular rotation relative to the underlying flow over the time-interval $[t_0, t_N]$ cf a trajectory starting at \mathbf{x}_0 . In order for $\mathbf{v}(\mathbf{x}(t), t)$ to evolve as a nearly material vector along a trajectory $\mathbf{x}(t)$, the Lagrangian acceleration $\mathbf{a}(t) := \ddot{\mathbf{x}}(t)$ must dominate the unsteady component of the velocity field:

$$|\frac{\partial \mathbf{v}(\mathbf{x}(t), t)}{\partial t}| \ll |\ddot{\mathbf{x}}(t)| \quad (9)$$

Condition 9 relates to the fact that Lagrangian time scales dominate Eulerian time scales. This has been numerically verified on a two-dimensional, satellite-altimetry-derived ocean-surface current product (AVISO) in [26] and confirmed in several experimental studies also on surface drifters [12, 58, 33]. Additionally, in order for $\overline{\text{TRA}}$ to be an adiabatically quasi-objective scalar field (i.e. approximate; an objective scalar field), the Lagrangian acceleration needs to dominate the angular acceleration of the trajectory induced by the spatial mean vorticity. This assumption has been found to hold on large enough flow domains in the ocean [23, 1, 6, 25].

We associate to the trajectory $\mathbf{x}(t; \mathbf{x}_0, t_0) := \mathbf{x}(t)$ over the time-interval $[t_0, t_N]$ its corresponding $\overline{\text{TRA}}$ value. Reconstructing the $\overline{\text{TRA}}$ field from sparse drifter trajectories via scattered interpolation allows visualization of vortical

flow structures without introducing ad-hoc tunable parameters. As vortices tend to be elliptic geometric objects, we use linear radial basis function interpolation which favors such structures. Local maxima in the TRA field are related to areas of high material rotation and hence indicate underlying rotational flow features.

3.2 Trajectory length

The trajectory length is a single trajectory Lagrangian diagnostic, which aims to reconstruct LCSs and which can potentially be applied to a sparse set of material trajectories [36, 37]. However, as pointed out by [53, 54], it is inherently non-objective and its relation to material features is unclear. The trajectory length is given by the arc-length of the trajectory $\mathbf{x}(t)$ over the time-interval $[t_0, t_N]$ starting at \mathbf{x}_0 :

$$M_{t_0}^{t_N}(\mathbf{x}_0) = \sum_{i=0}^N |\dot{\mathbf{x}}(t_i)| \quad (10)$$

In an attempt to visualize elliptic LCSs from a set of sparse drifter data, we reconstruct the trajectory length diagnostic over a broader domain using linear radial basis function interpolation. [36, 37] suggest that dynamical regions in the flow are separated by abrupt variations in the arc length function and that oceanic eddies are characterized by inner cores of minimal trajectory length value surrounded by closed contours with high spatial gradients.

3.3 Automatic looper detection

Based on the natural idea of considering looping trajectories a characteristic footprint of coherent Lagrangian eddies, [63, 18, 13, 35] extracted looping drifter segments from the Lagrangian spin

$$\Omega(t_i) = \frac{\langle \mathbf{e}_z, \dot{\mathbf{x}}(t_i) \times \ddot{\mathbf{x}}(t_i) \rangle}{\frac{1}{2} \sum_{i=0}^N |\dot{\mathbf{x}}(t_i)|^2}, \quad (11)$$

first introduced in [56]. The term $\frac{1}{2} \sum_{i=0}^N |\dot{\mathbf{x}}(t_i)|^2$ corresponds to the average eddy kinetic energy and $\mathbf{e}_z = (0, 0, 1)^T$. Ω quantifies the rotation of the velocity vector and is physically related to the vorticity. Evaluating eq. 11 along a Lagrangian particle trajectory provides an overall measure of rotation within a time series over the time-interval $[t_0, t_N]$. Looping segments of a trajectory are characterized as intervals between zero crossings of Ω . The duration of each segment of sustained positive or negative Ω is denoted as the persistence. For each segment, we define the period P :

$$P = \frac{2\pi}{|\Omega^*|}, \quad (12)$$

where $|\Omega^*|$ is the absolute value of the median of Ω over the segment. Looping segments are defined as trajectory intervals where the persistence exceeds two times the period P . This threshold value was proposed in [35].

3.4 Lagrangian averaged vorticity deviation

[24] introduced an objective Lagrangian vortex identification diagnostics based on rotational coherence in the flow. Similarly to the TRA, the Lagrangian averaged vorticity deviation (LAVD) characterizes the local material rotation in the flow via a trajectory-based rotation metric. Computing the LAVD value associated to a trajectory $\mathbf{x}(t; \mathbf{x}_0, t_0)$ over the time-interval $[t_0, t_N]$, however, requires evaluating the vorticity

$$\omega(\mathbf{x}(t), t) = \nabla \times \mathbf{v}(\mathbf{x}(t), t)$$

along the particle trajectories:

$$\text{LAVD}_{t_0}^{t_N}(\mathbf{x}_0) = \frac{1}{t_N - t_0} \int_{t_0}^{t_N} |\omega(\mathbf{x}(s), s) - \overline{\omega(s)}| ds. \quad (13)$$

where

its computation requires
the knowledge of the velocity field
over a large enough domain.
Therefore, even

$\bar{\omega}(t)$ denotes the spatially averaged vorticity at time t . Even though the LAVD is a quantity associated to a single particle trajectory, in order to compute the vorticity a densely gridded velocity dataset is required. This renders the LAVD method inapplicable to arbitrary sparse drifter data. However, the LAVD has been used in a variety of works to visualize and extract vortices from densely gridded ocean velocity datasets [24, 1, 7]. Local maxima in the LAVD field surrounded by nested closed and nearly convex level curves are related to rotational flow features. In this work, we apply the LAVD method to the AVISO data and compare the vortical features resulting from the geostrophic velocity field with those given by the TRA computed from drifter data.

4 Results

4.1 Grand LAgrangian Deployment (GLAD)

Drifters released as part of the GLAD experiment have mostly been used to study statistical dispersion properties of the ocean over a wide range of scales [47, 5, 38]. Furthermore, [46] and [45] showed that there is moderate agreement between the evolution of the drifters and nearby attracting LCSs extracted from the geostrophic velocity field. Specifically, drifter behavior agreed with the *tiger tail* pattern inferred from the chlorophyll distribution shown in Fig. 1. The chlorophyll plume extended over more than 100 kilometres and coincided with an attracting LCS [45]. Drifters in proximity of the tip of the tiger tail organized themselves into long filaments along the chlorophyll plume. Some of the drifters (in red) additionally exhibited some degree of clustering, suggesting the presence of an elliptic LCS close to the chlorophyll front. Here we seek to visualize vortices by reconstructing the TRA field from drifter data over the interval [222doy, 229doy] using linear radial basis function interpolation. The TRA, shown in Fig. 2, is plotted with respect to the final drifter positions at time $t = 229$ doy. It uncovers two major rotational features marked by high values of TRA. For comparison, we include three further Lagrangian trajectory metrics: the LAVD computed from geostrophic velocity currents, the trajectory length and the looping segments computed from drifter data.

4.1.1 Coastal area

I would say three

This plot reveals
Eddy diagnostics

We start by focusing on the area at the outlet of the Mississippi river. Coastal flows are regions of intense mixing [3], often characterized by high potential vorticity and strong horizontal shear, which are responsible for the formation of small-scale eddies [59, 60]. Evidence for the existence of submesoscale elliptic features and strong mixing areas on the continental shelf is also found in the TRA (Fig. 2a). Furthermore, anticyclonic looping segments extracted from the automated looper extraction method, confirm the presence of small scale vortices at the outlet of the Mississippi river (Fig. 2f). In contrast, the trajectory length diagnostic provides no indication of elliptic features in coastal flow areas (Fig. 2b). We recall that vortical flow features in the arclength field are visible as local minima surrounded by closed contours with abrupt variations. In coastal areas the trajectory length uniformly attains low values, thereby indicating that drifters trapped in coastal areas do not travel long distances. There exists, however, no physically justified relation between the distance travelled by surface drifters and vortical flow features. The LAVD displays uniformly low values close to the outlet of the Mississippi river and therefore does not succeed in highlighting coastal eddies (Fig. 2b). We attribute the mismatch between the LAVD and the TRA to the fact that the geostrophic velocity field is not a good approximation of the true underlying ocean surface velocity close to the outlet of the Mississippi river. We conclude that in coastal areas, the drifter-based TRA captures the flow dynamics with much higher detail than the AVISO-based LAVD.

4.1.2 Mesoscale eddy

The TRA highlights another strongly rotational area close to the chlorophyll plume extending from the outlet of the Mississippi river to the open ocean (Fig. 2a) at (87.5°E, 27°N). The prominent clustering of the drifters and the cyclonic looping segments confirm the presence of such a mesoscale eddy (Fig. 2d). The automated looper extraction algorithm is a powerful methodology which allows to efficiently extract looping trajectory segments. However, it requires the manual tuning of threshold parameters. Contrarily, the TRA allows a parameter-free visualization of vortical flow structures from sparse drifter data. The investigated elliptic LCS is also visible in the LAVD, which

THERE SEEMS TO BE
REGION #3 OF HIGH
VALUES

I would not say bad. It seems
to have lower values is not
very

I would say two stark

ARE THERE SEVERAL OF THEM?
DESCRIBE IN SECTION 3.3
HOW THEY HAVE TO BE TUNED

DO WE EQUALLY STRICTLY ENFORCE A CRITERION FOR TRA AND LOOPING?
MY IMPRESSION IS THAT WE ARE JUST LOOKING AT REGIONS
OF HIGHS AND LOWS FOR THE TRA, AS APPROVED TO
EXTRACTING MAXIMA WITH CLOSED LOWS. IF THIS IS NOT SO,
THE TEXT SHOULD BE MORE EXPLICIT ABOUT THIS.

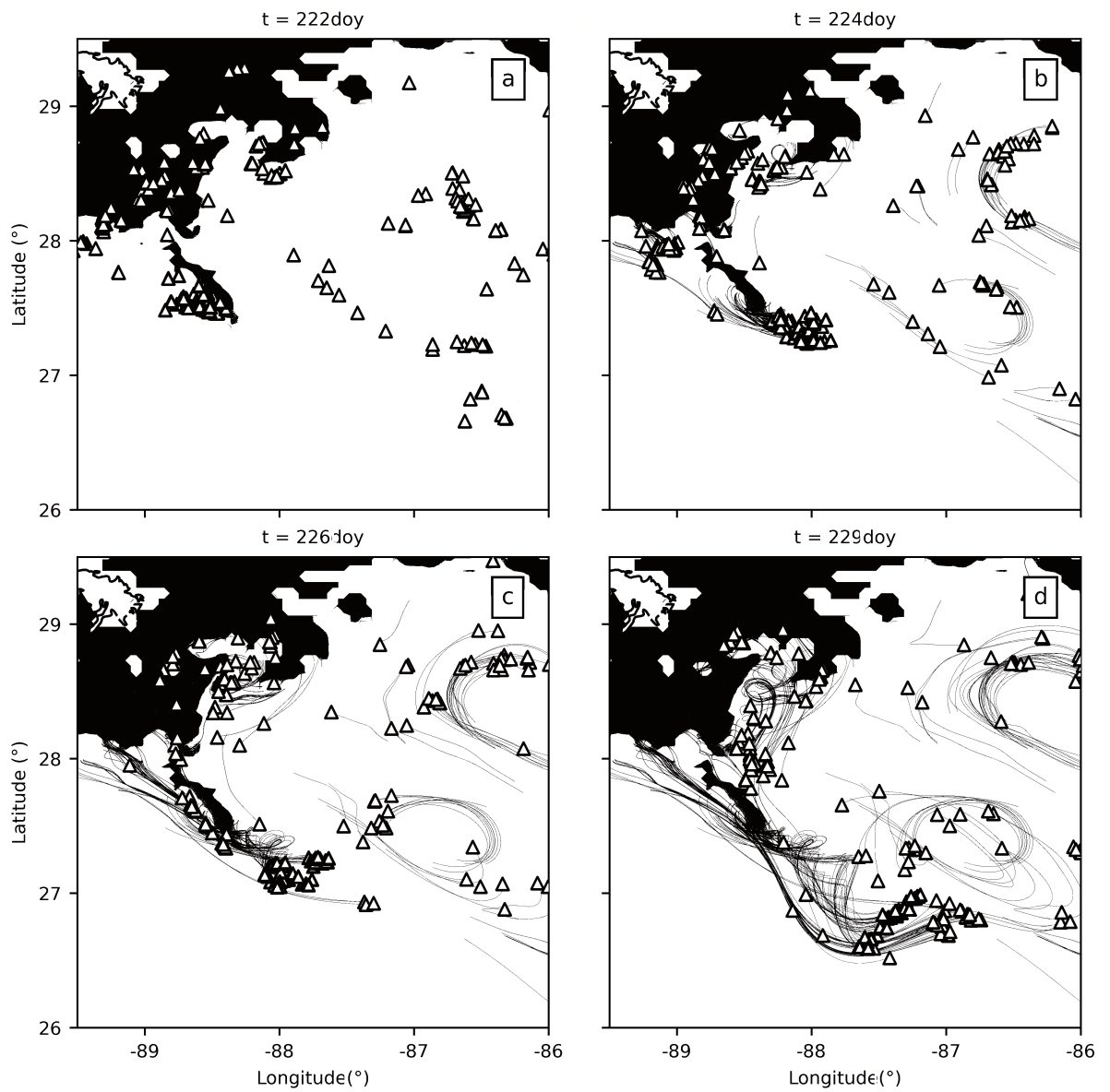


Figure 1: Evolution of GLAD-drifters overlayed on 8-day composite chlorophyll-a concentration (12 August, 2012). Most drifters (white triangles) formed a long filament along the chlorophyll plume extending deep into the Gulf of Mexico. Drifters additionally forming a visible tight cluster are colored in red. The blue cross denotes the outlet of the Mississippi river.

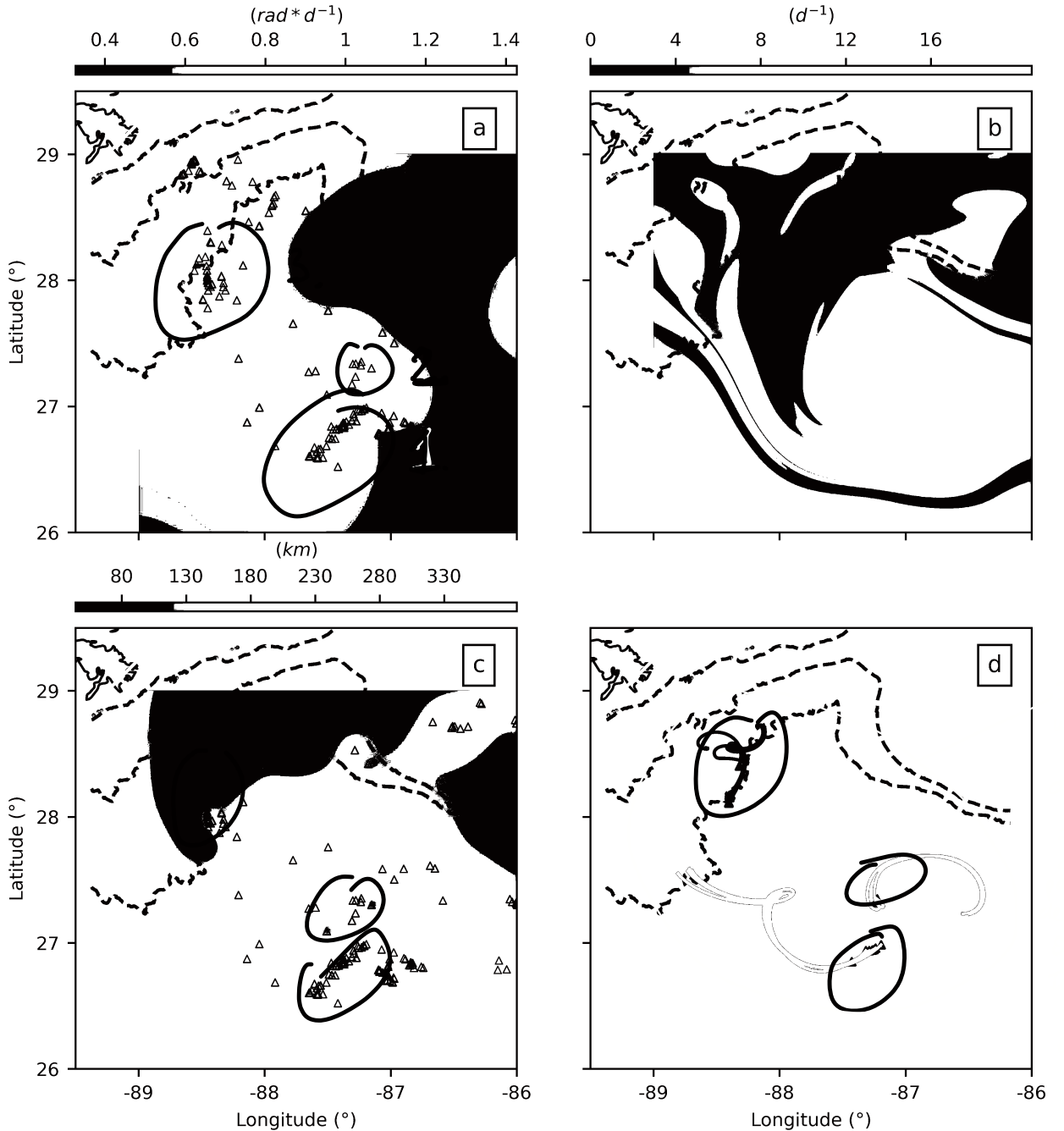


Figure 2: The dashed black lines correspond to the isobaths (-100m , -1000m , -2000m). The blue cross coincides with the outlet of the Mississippi river. (a) Reconstructed $\overline{\text{TRA}}_{222}^{229}$ field plotted with respect to the position of the drifters (triangles) at time $t = 229\text{day}$. (b) LAVD_{222}^{229} field computed from AVISO plotted at time $t = 229\text{day}$. (c) Reconstructed M_{222}^{229} field plotted with respect to the position of the drifters (triangles) at time $t = 229\text{day}$. (d) Cyclonic (red) and anticyclonic loopers computed according to [35].

are also present but less pronounced in the trajectory length diagnostic.

Is it true that it has no closed level curves over the minima, whereas the TRA does have closed level curves around maxima? If yes, this needs to be illustrated. same for the Lagrangian spin.

displays a nearly circular and swirling feature with distinguishable high values (Fig. 2b). On the contrary, the features resulting from the arclength diagnostic are ~~more~~ less pronounced (Fig. 2c). The rotational feature under investigation displays low arclength values. There exists, however, no distinguishable sharp and closed boundary with abrupt variations which could suggest the presence of an elliptic LCS. The TRA, the LAVD and the automated looper extraction method from [35], all ~~strongly~~ agree on the presence of a vortical flow structure located at (87.5°E, 27°N) at time $t = 229$ doy, whereas the trajectory length diagnostic provides an inconclusive picture.

4.1.3 Quasi-material advection

In order to further verify and investigate the ~~vertical flow structures~~ inferred from the TRA, we proceed by quasi-materially advecting the ~~TRA~~ distribution over the time-interval [222doy, 229doy] (see Fig. 3). Truly material ~~advection would require~~ ~~spatially and temporally~~ ~~well-defined~~ velocity field. In ~~this sparse~~ ~~our setting~~, however, the velocity field is only sparsely known and hence the advected structures are inherently non-material: At every time step, the ~~TRA~~ must be approximated from the current drifter distribution, using linear radial basis interpolation. However, the ~~TRA~~²²⁹-distribution approximates a materially advected frame-indifferent scalar quantity as it is reconstructed based on truly materially evolving drifter trajectories. Therefore, we refer to it as ~~quasi-material~~ *term already used and explained* ~~advection~~.

Nevertheless,

described

Fig 3 displays the quasi-material evolution of the ~~TRA~~ as drifters are advected forward in time over the time-interval [222doy, 229doy]. Additionally, the closed white curves indicate eddy boundaries extracted from the ~~TRA~~ using the algorithm proposed in Appendix A. The red closed curve denotes the materially advected vortex boundary extracted from the LAVD at time $t = 229$ doy using the algorithm introduced in [24]. Eddy boundaries are viewed as outermost (almost) convex contours around a local maximum in the LAVD field. Hence, the algorithm requires specifying three parameters: the minimum length l_{min} of the perimeter of the eddy, the convexity deficiency c_d and the minimum allowed local maximum $\overline{\text{LAVD}}_{loc,max}$. In the following example we set $l_{min} = 50\text{km}$, $c_d = 10^{-4}$ and $\overline{\text{LAVD}}_{loc,max} = 0.5\overline{\text{LAVD}}_{max}$, where $\overline{\text{LAVD}}_{max}$ is the global maximum of the LAVD in the chosen domain. Similarly, the ~~TRA~~-based eddy boundary extraction algorithm requires finding convex closed curves surrounding a local maximum in the ~~TRA~~ field satisfying a set of conditions (see Appendix 1 for further details). As in the case of the LAVD, there are three parameters involved here: the minimum length l_{min} of the perimeter of the eddy; the minimum number of drifters inside the eddy n_d and the minimum allowed local maximum $\overline{\text{TRA}}_{loc,max}$. For the following example, the chosen parameters are $l_{min} = 50\text{km}$, $n_d = 5$ and $\overline{\text{TRA}}_{loc,max} = 0.5\overline{\text{TRA}}_{max}$, where $\overline{\text{TRA}}_{max}$ is the global maximum of the ~~TRA~~ in the chosen domain. The eddy boundary inferred from AVISO data at $t = 229$ doy is materially advected using the geostrophic velocity field $\mathbf{v}_g(\mathbf{x}, t)$, whereas the eddy boundaries inferred from the drifter-based ~~TRA~~²²⁹ are quasi-materially advected based on the evolving drifter trajectories.

At $t = 222$ doy, the ~~TRA~~ suggests the presence of several small-scale vortices at the outlet of the Mississippi river and at open sea (see Fig. 3a). The submesoscale eddies close to the outlet of the Mississippi river remain trapped in coastal areas and eventually merge into a larger vortical flow feature. Over the time-interval [222doy, 229doy], the LAVD-based eddy does not coincide with any of the eddies inferred from the TRA (Fig. 3a-d). The white eddy initially located at approximately (88.5°W, 27.5°N) is associated to the clustered red drifters identified in Fig. 1, thereby confirming the existence of the submesoscale eddy along the chlorophyll front. This agrees with the observation put forward in [46] [45]. The eddy develops along the chlorophyll plume and then slowly detaches from it. The extracted eddy barriers ~~moderately well inhibit~~ *limit* the transport of particles between the interior and the exterior of the eddy. Hence, vortical flows structures generated along oceanic fronts represent a possible transport route for inertial particles as they can carry material over long distances away from the front.

4.1.4 Vortex merging merger

in Fig. 3

The two submesoscale eddies initially located at (88.5°W, 27.5°N) and (86.5°W, 27.25°N) eventually merge approximately at time $t = 228$ doy to form a larger mesoscale eddy. Towards the end of the advection process, the ~~vortical flow feature~~ suggested by the LAVD coincides with the eddy inferred from the drifter-based ~~TRA~~. The formation and evolution of the mesoscale eddy, however, is clearly different. The red eddy shows no degree of filamentation and,

elliptic LCS

highlighted

, as any other Lagrangian diagnostic

merges of

full

This is probably not needed

expected remains coherent over the complete time-interval [222doy, 229doy]. The white eddy at $t = 229$ doy results from the ~~vortex merging between~~ two smaller submesoscale eddies and is visibly larger than the red eddy. ~~Vortex merging is a frequently discussed phenomenon in the ocean, where two (or more) small scale eddies merge into a larger vortical flow structure [10, 10, 51]~~ As the LAVD based eddy boundary is a purely materially advected closed curve, per definition it can neither split nor merge with any other materially advected curve. Hence, by construction, the LAVD is not able to capture the ~~vortex merging~~. Contrarily, the quasi-materially advected TRA-based eddy boundaries can merge into larger eddies. This follows from the fact, that the computation of the eddy boundary from the TRA distribution is independently carried out at each and every time step. Despite, the minimal amount of data, the TRA reveals features, which are hidden in the AVISO-based LAVD. Furthermore, we have shown that the TRA, more effectively characterizes eddies than other commonly used single trajectory rotation metrics.

4.2 Global Drifter Program (GDP)

In our second example, we focus on a set of drifters in the western North-Atlantic. This oceanic region is characterized by a strong and persistent formation of eddies arising from the meanders of the Gulf Stream [27, 49]. On the 4th of October, 2006, a floating sargassum patch was detected by the Medium Resolution Imaging Spectrometer (MERIS) on Envisat. This feature has a spiralling shape that is also visible from satellite-altimetry data [4]. This floating sargassum patch is visualized in Fig. 4b using the Maximum Chlorophyl Index (MCI) [9]. Due to persistent cloud-coverage, such clear snapshots of floating material in the ocean are very rare and hence one can additionally take advantage of surface drifter observations.

In the following we use the TRA to extract the eddy highlighted by the spiralling sargassum patch described in [4]. For comparison purposes, we additionally include two further single-trajectory metrics: the trajectory length diagnostic (see Fig. 4f) and the looping segments computed according to [35] (see Fig. 4d). We avoid evaluating the satellite altimetry-based LAVD, and instead include a direct snapshot of the floating sargassum patch which clearly indicates the presence of a vortical flow feature (see Fig. 4b). Similarly to the MCI, the TRA reveals the presence of a Lagrangian eddy centered at around (68°W, 37.5°N). As the physical intuition suggests, this eddy is visible as a distinguished local maximum in the TRA field. The white eddy boundary is extracted from the TRA using the algorithm proposed in Appendix A by setting $l_{min} = 50\text{km}$, $n_d = 2$, $\text{TRA}_{loc,max} = 0.5\text{TRA}_{max}$. The extracted eddy boundary underestimates the size of the sargassum patch, but approximates the location (Fig. 4b). The cyclonic looping exhibited by the two trajectories inside the eddy additionally confirms the presence of an elliptic LCS (Fig. 4d). The trajectory length diagnostic displays a feature similar to the TRA (Fig. 4f). The prominent local maximum in the arclength function, indicates that drifters in this area exhibit clearly distinct trajectory behaviour compared to the drifters in the rest of the flow domain. However, whether or not this suggests the presence of an elliptic LCS is debatable. We recall that elliptic LCS are supposedly visible as local minima in the trajectory length diagnostic. The shown example clearly contradicts this statement as the eddy is close to a local maximum of the arclength function. Hence, as opposed to the TRA, the trajectory length diagnostic leads to contradictory conclusions about underlying vortical flow structures. We have thus shown that, compared to existing single trajectory diagnostics, the TRA computed from sparse drifter data provides spatially resolved details of transport barriers at high fidelity and precision. This approach is free from the limitation of remote sensing data, which require careful preprocessing to eliminate the impacts of external factors, such as cloud coverage. As opposed to the automated looper extraction algorithm, the TRA allows a parameter free visualization of vortical flow structures by retaining all trajectory data and associating to each and every drifter trajectory a Lagrangian diagnostic related to the material rotation in the flow.

5 Conclusion

Lagrangian eddies (elliptic LCSs) are material objects responsible for the transport of floating particles over large distances in the ocean. They are, by definition, frame-indifferent and thus can only be reliably characterized with objective feature extraction methods. The local ocean velocity is most accurately observed from float trajectory data, which, however, is inherently non-objective, representing an inconsistency that available eddy detection methods for sparse trajectories do not address. Those methods typically describe eddies by extracting the looping segments of a

(*) New paragraph:

The trajectory-length diagnostic shows a nearly maximum, which is inconsistent with the footprint generally envisaged for a coherent eddy in the M₁₀ field (see Fig. 4c)
The trajectory-length diagnostic shows a nearly maximum, which is inconsistent with the footprint generally envisaged for a coherent eddy in the M₁₀ field
(see section 3.2).

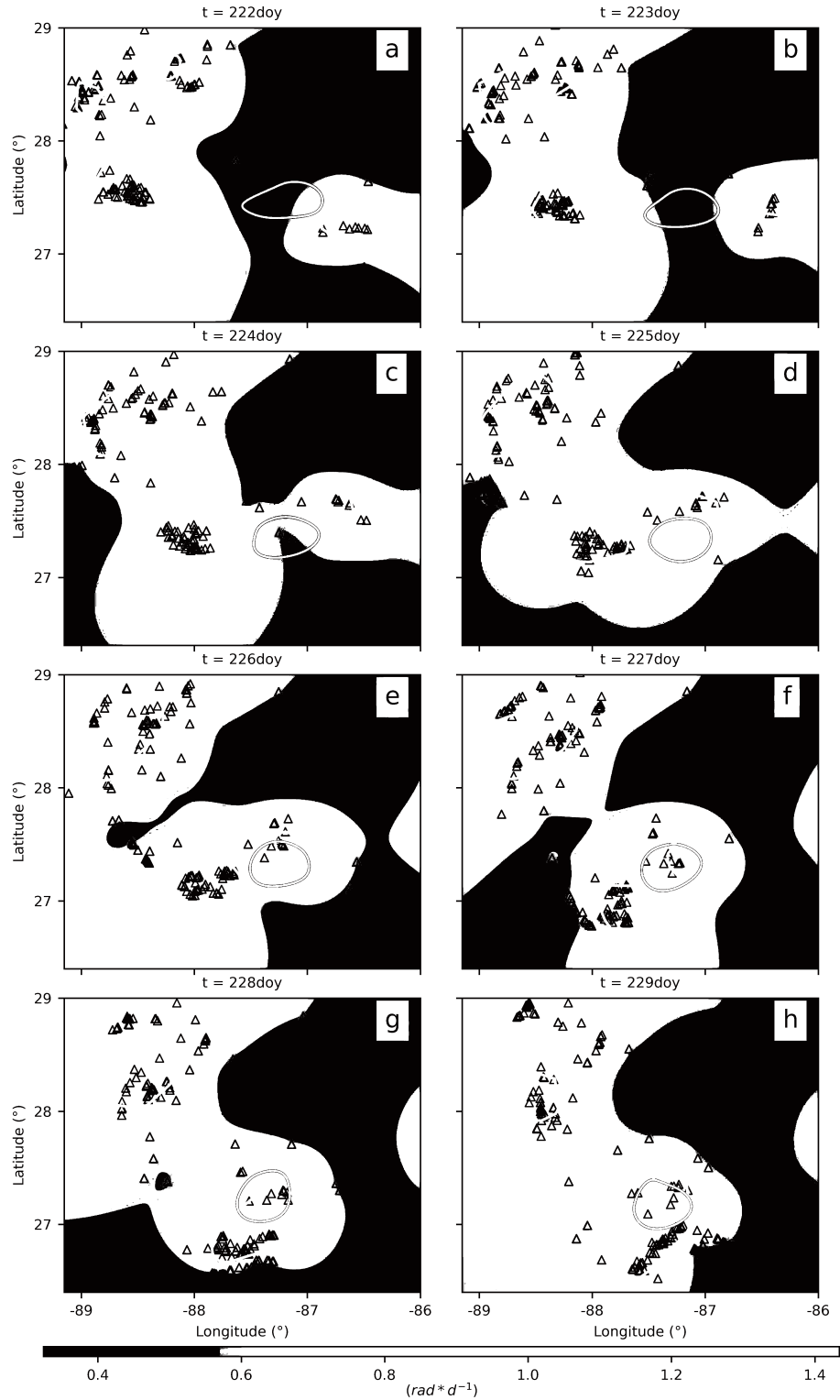


Figure 3: Quasi materially advected $\overline{\text{TRA}}_{222}^{229}$ for the GLAD dataset. Closed white curves display eddy boundaries extracted from the drifter based $\overline{\text{TRA}}$ using the algorithm proposed in Appendix A. Closed red curves indicate eddy boundaries obtained from the AVISC based LAVD computation. Triangles indicate the position of the drifters at time t .

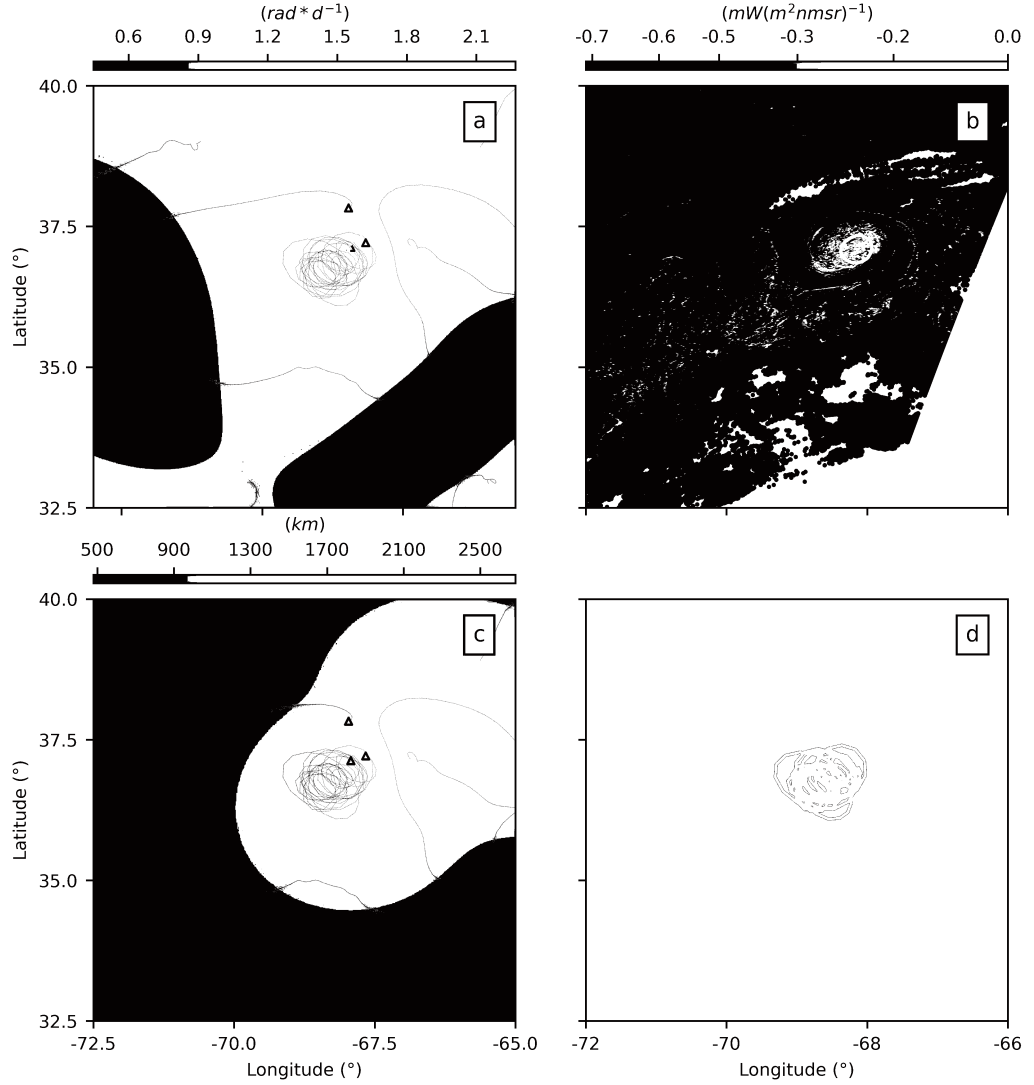


Figure 4: (Left) (a) Reconstructed $\overline{\text{TRA}}_{246}^{276}$ field plotted with respect to the position of the drifters (triangles) at time $t = 276\text{doy}$. (b) Eddy boundary superimposed on the floating sargassum concentration inferred from the Maximum Chlorophyl Index (MCI) at $t = 276\text{doy}$. Regions covered by clouds are displayed in white. (c) Reconstructed M_{246}^{276} field plotted with respect to the position of the drifters (triangles) at time $t = 276\text{doy}$. (d) Cyclonic (red) loopers computed according to [35].

trajectory, but their definition of looping depends on the frame of the observer. Furthermore, looping segments of a trajectory are most commonly described by these methods in a statistical sense and hence are not geared towards highlighting individual Lagrangian eddy boundaries with high accuracy.

In this paper, we have proposed to tackle this inconsistency from a dynamical systems perspective by applying the adiabatically quasi-objective $\overline{\text{TRA}}$ diagnostic [25, 26] to sparse drifter datasets. The $\overline{\text{TRA}}$ field approximates objective material rotation measure in frames satisfying specific conditions that generally hold in the ocean. We have found that vortical flow features are related to regions of high local material rotation. Hence, they can be identified as local maxima in the $\overline{\text{TRA}}$ field. The $\overline{\text{TRA}}$ highlights both submesoscale and mesoscale vortices from sparse drifter data, as demonstrated in the two examples. Furthermore, it also succeeds in characterizing the mixing and stirring processes in coastal flow regions and correctly characterizes the merger of two originally distinct eddies. Contrary to existing single trajectory diagnostics, both the $\overline{\text{TRA}}$ and the LAVD are physically related to the local material rotation in the flow. Compared to the LAVD, which correctly highlights vortical flow features given a sufficiently densely gridded velocity dataset, the $\overline{\text{TRA}}$ can be applied to arbitrarily sparse drifter data. Hence, it allows incorporating valuable drifter data into the analysis of oceanic coherent structures in a physically and mathematically justifiable sense. This proves to be especially useful in ocean regions, where satellite altimetry based data does not succeed in unravelling the true underlying ocean flow dynamics. The looper segments extracted using the algorithm proposed in [35] coincide with the features identified in the $\overline{\text{TRA}}$. However, a spaghetti plot of looping trajectory segments does not help in identifying transport barriers and eddy boundaries. With increasing amount of drifter data, plotting a series of individual looping segments leads to confusing and unclear eddy visualizations. Furthermore, potentially valuable information is lost when discarding non-looping trajectory segments based on a manually tuned threshold parameter. The $\overline{\text{TRA}}$ does not suffer from this limitation as it allows visualizing flow features via a scalar field without explicitly relying on user defined threshold parameters.

Apart from the visual inspection of the reconstructed $\overline{\text{TRA}}$ field, we have additionally presented an algorithm to extract approximate eddy boundaries from sparse drifter data. As vortical flow features are indicated by blobs close to local maxima in the $\overline{\text{TRA}}$ field, the proposed method resembles a blob detection algorithm, thereby inherently relying on predefined parameters. Passing from a continuous scalar diagnostic field to a set of closed curves, inevitably requires introducing user-defined parameters. All in all, however, the number of free parameters is comparable to other multi-trajectory Lagrangian eddy detection methods [24, 61]. This is noteworthy as these algorithms were originally designed assuming knowledge of the underlying velocity field.

This work represents one of the first attempts to apply a physically justifiable Lagrangian diagnostic quantity to a sparse set of drifter data. We compared the outcome of several commonly used single particle trajectory diagnostics over dynamically distinct datasets and find that the $\overline{\text{TRA}}$ most effectively characterizes vortical flow features in a sparse data context. Hence, the method developed here shows promise of general applicability to drifter datasets.

A Eddy Boundary Extraction Algorithm

Available eddy extraction algorithms are presented in [64, 20, 23, 57]. These methods, however, assume trajectory density that is generally unavailable for drifter trajectories in the ocean. Here, we propose an algorithm that extracts approximate eddy boundaries from the topology of the reconstructed $\overline{\text{TRA}}$ field. Intuitively, vortices are identified by this algorithm as blobs close to local maxima in the $\overline{\text{TRA}}$ field.

Passing from a continuous scalar field to a set of discrete closed curves, representative of eddy boundaries, inevitably requires introducing threshold parameters. There are three main parameters involved in Algorithm 1. The first user-defined quantity involves the identification of the local maxima in the $\overline{\text{TRA}}$ field. As we identify vortical flow features with regions of high $\overline{\text{TRA}}$, local maxima below a predefined threshold $\overline{\text{TRA}}_{\text{loc},\max}$ are neglected. Additionally, we also need to specify the minimum number of drifters n_d inside an eddy. As elliptic LCS are often observed via a dense clustering of floatsam, this parameter is generally set to be greater than 1. In general, n_d should vary depending on the sparsity of float trajectory data. The third parameter involves putting a threshold on the minimum length of the final eddy boundary l_{\min} in order to filter out unrealistically small eddies.

Algorithm 1 Extraction of approximate eddy boundaries from $\overline{\text{TRA}}_{t_0}^{t_N}$ – field

Input: Trajectories over the time-interval $[t_0, t_N]$.

1. Reconstruct $\overline{\text{TRA}}_{t_0}^{t_N}$ field at time t using linear radial basis interpolation. Depending on the noise levels in the data, the resulting $\overline{\text{TRA}}_{t_0}^{t_N}$ field can additionally be smoothed.
2. Find local maxima of $\overline{\text{TRA}}_{t_0}^{t_N}$ which are above a threshold $\overline{\text{TRA}}_{\text{loc}, \max}$.
3. Compute for each closed level set surrounding a local maximum, the median of $|\nabla \overline{\text{TRA}}_{t_0}^{t_N}|$: $|\nabla \overline{\text{TRA}}_{t_0}^{t_N}|$ varies for each point on the closed level set. However, we need to associate to each closed level set a unique representative quantity for $|\nabla \overline{\text{TRA}}_{t_0}^{t_N}|$. Frequently used statistical estimators are for instance the median and the mean. In a practical setting, we prefer to choose the median as it is more robust with respect to outliers and noise than the mean.
4. Find closed level set with the maximum median of $|\nabla \overline{\text{TRA}}_{t_0}^{t_N}|$ which additionally
 - (a) has at least one local maximum of $\overline{\text{TRA}}_{t_0}^{t_N}$ in its interior.
 - (b) contains at least n_d -trajectories.
5. Take the convex hull of all the selected closed curves.
6. If two or more convex closed curves intersect, then take union of these curves.
7. Take the convex hull of the resulting closed curves.
8. Require that the perimeter of the eddy boundary is at least greater than l_{\min} .

Output: Approximate eddy boundaries at time t .

The choice of the parameters inevitably influences the number and size of the extracted eddies. By construction, the extracted eddy boundaries are closed convex curves characterized by sharp gradients. They do not necessarily coincide with closed level sets of the $\overline{\text{TRA}}$. Most of the involved parameters are conceptually similar to the ones employed in the LAVD-based eddy boundary extraction algorithm. The methodology applies both to sparse and densely gridded data.

Data Availability

The AVISO geostrophic current velocity product used in this study, "Global Ocean Gridded L4 Sea Surface Heights and Derived Variables Reprocessed," is freely available and is hosted by the Copernicus Marine Environment Monitoring Service (<http://marine.copernicus.eu>). The LAVD computations have been carried out with the software TBarrier. Jupyter notebooks (together with further drifter data) implementing the methods described are shared in an online repository at Github/EncinasBartos. The codes performing the drifter data preprocessing have also been included. Hence, these codes can readily be applied to any sparse trajectory dataset.

References

- [1] R. Abernathey and G. Haller, "Transport by lagrangian vortices in the eastern pacific," *Journal of Physical Oceanography*, **48.3** (2018): 667-685.
- [2] R. Abernathey, C. Bladwell, G. Froyland, and K. Sakellariou, "Deep Lagrangian connectivity in the global ocean inferred from Argo floats," *Journal of Physical Oceanography*. (2021)
- [3] N. Aksamit, T. Sapsis, G. Haller, "Machine-Learning Mesoscale and Submesoscale Surface Dynamics from Lagrangian Ocean Drifter Trajectories," *Journal of Physical Oceanography*, **50** (2020) 1179–1196.
- [4] F. J. Beron-Vera, M.J. Olascoaga, G. Haller, M. Farazmand, J. Triñanes, and Y. Wang, "Dissipative inertial transport patterns near coherent Lagrangian eddies in the ocean," *Chaos: An Interdisciplinary Journal of Nonlinear Science*, **25** (2015), 087412.
- [5] F.J. Beron-Vera, and J.H. LaCasce, "Statistics of simulated and observed pair separations in the Gulf of Mexico," *Journal of Physical Oceanography*, **46** (2016), 2183–2199.
- [6] F. J. Beron-Vera, A. Hadjighasem, Q. Xia, M.J. Olascoaga, M. J., and G. Haller, "Coherent Lagrangian swirls among submesoscale motions," *Proceedings of the National Academy of Sciences*, **(116)** (2019) 18251–18256.
- [7] F. J. Beron-Vera and P. Miron, "A minimal Maxey-Riley model for the drift of Sargassum rafts," *Journal of Fluid Mechanics*, **904** (2020).
- [8] M. Berta, A. Griffa, M.G. Magaldi, T.M. Özgökmen, A.C. Poje, A.C. Haza and M.J. Olascoaga, "Improved surface velocity and trajectory estimates in the Gulf of Mexico from blended satellite altimetry and drifter data.," *Journal of Atmospheric and Oceanic Technology*, **(10)**, (2015) 1880-1901.
- [9] C. E. Binding, T.A. Greenberg, R.P. Bukata, "The MERIS maximum chlorophyll index; its merits and limitations for inland water algal bloom monitoring," *Journal of Great Lakes Research*, **39** (2013), 100–107.
- [10] C. Cerretelli, and C. H. K. Williamson, "The physical mechanism for vortex merging," *Journal of Fluid Mechanics*, **475** (2003), 41-77.
- [11] D.B. Chelton, G.S. Michael, M.S. Roger, and R. A. de Szoeke, "Global observations of large oceanic eddies," *Geophysical Research Letters* **34**(2007).
- [12] R. E. Davis, "Drifter observations of coastal surface currents during CODE: The method and descriptive view," *Journal of Geophysical Research: Oceans*, **90** (1985), 4741–4755.

- [13] C. Dong, Y. Liu, R. Lumpkin, M. Lankhorst, D. Chen, J.C. McWilliams and Y. Guan, "A scheme to identify loops from trajectories of oceanic surface drifters: An application in the Kuroshio Extension region," *Journal of Atmospheric and Oceanic Technology*, **28** (2011), 1167-1176.
- [14] J. H. Faghmous, I. Frenger, Y. Yao, R. Warmka, A. Lindell and V. Kumar, "A daily global mesoscale ocean eddy dataset from satellite altimetry," *Scientific data*, **2** (2015), 1-16.
- [15] G. Froyland, R.M. Stuart and E. van Sebille, "How well-connected is the surface of the global ocean?" *Chaos: An Interdisciplinary Journal of Nonlinear Science*, **24** (2014), 033126.
- [16] G. Froyland and K. Padberg-Gehle, "A rough-and-ready cluster-based approach for extracting finite-time coherent sets from sparse and incomplete trajectory data," *Chaos: An Interdisciplinary Journal of Nonlinear Science*, **25** (2015), 087406.
- [17] A. Griffa, "Applications of stochastic particle models to oceanographic problems," *Stochastic modelling in physical oceanography* (pp. 113–140)(1996).
- [18] A. Griffa, A., Lumpkin, R., and Veneziani, M. Cyclonic and anticyclonic motion in the upper ocean. *Geophysical Research Letters*, **35** (2008).
- [19] J. Gula, M.J. Molemaker and J.C. McWilliams, "Submesoscale dynamics of a Gulf Stream frontal eddy in the South Atlantic Bight," *Journal of Physical Oceanography*, **46** (2016), 305-325.
- [20] A. Hadjighasem, D. Karrasch, H. Teramoto and G. Haller, "Spectral-clustering approach to Lagrangian vortex detection," *Physical Review E*, **93** (2016), 063107.
- [21] A. Hadjighasem, M. Farazmand, D. Blazevski, G. Froyland and G. Haller, "A critical comparison of Lagrangian methods for coherent structure detection," *Chaos: An Interdisciplinary Journal of Nonlinear Science*, **27(5)**, 053104.
- [22] G. Haller, Lagrangian coherent structures. *Ann. Rev. Fluid Mech.* **47** (2015) 137-162.
- [23] G. Haller, "Dynamically consistent rotation and stretch tensors from a dynamic polar decomposition," *J. Mechanics and Physics of Solids*, **80** (2016) 70-93.
- [24] G. Haller, A. Hadjighasem, M. Farazmand and F. Huhn, "Defining coherent vortices objectively from the vorticity." *J. Fluid Mech.* **795** (2016) 136-173.
- [25] G. Haller, N.O. Aksamit, and A. P. Encinas-Bartos, "Quasi-objective coherent structure diagnostics from single trajectories," *Chaos: An Interdisciplinary Journal of Nonlinear Science* **31** (2021).
- [26] G. Haller, N. Aksamit and A.P. Encinas-Bartos, Erratum: 'Quasi-objective coherent structure diagnostics from single trajectories' *Chaos: An Interdisciplinary Journal of Nonlinear Science* **31** (2021)
- [27] D. Kang and E.N. Curchitser, "Gulf Stream eddy characteristics in a high-resolution ocean model," *Journal of Geophysical Research: Oceans*, **118** (2013), 4474–4487.
- [28] M. Lévy, P.J. Franks and K.S. Smith, "The role of submesoscale currents in structuring marine ecosystems," *Nature communications*, **9** (2018), 1–16.
- [29] R. Lguensat, M. Sun, R. Fablet, P. Tandeo, E. Mason, and G. Chen, "EddyNet: A deep neural network for pixel-wise classification of oceanic eddies," *IGARSS 2018-2018 IEEE International Geoscience and Remote Sensing Symposium* (2018) (pp. 1764–1767). IEEE.
- [30] J. M.Lilly and S.C. Olhede, "Bivariate instantaneous frequency and bandwidth," *IEEE Transactions on Signal Processing*, **58** (2009), 591–603.
- [31] J. M.Lilly and S.C. Olhede, "On the analytic wavelet transform," *IEEE transactions on information theory*, **56(8)**, 4135-4156.

- [32] J. M. Lilly and P. Pérez-Brunius, "Extracting statistically significant eddy signals from large Lagrangian datasets using wavelet ridge analysis, with application to the Gulf of Mexico," *Nonlinear Processes in Geophysics*, **28** (2021), 181–212.
- [33] R. Lumpkin, A. M. Treguier and K. Speer, "Lagrangian eddy scales in the northern Atlantic Ocean," *Journal of physical oceanography*, **32**(9) (2002), 2425-2440.
- [34] R. Lumpkin and M. Pazos, "Measuring surface currents with Surface Velocity Program drifters: the instrument, its data, and some recent results," *Lagrangian analysis and prediction of coastal and ocean dynamics*, **39** (2007), 67.
- [35] R. Lumpkin, "Global characteristics of coherent vortices from surface drifter trajectories," *Journal of Geophysical Research: Oceans*, **121** (2016), 1306–1321.
- [36] C. Mendoza and A.M. Mancho, "Hidden geometry of ocean flows," *Physical review letters*, **105**(3) (2010), 038501.
- [37] A.M. Mancho, S. Wiggins, J. Curbelo and C. Mendoza, "Lagrangian descriptors: A method for revealing phase space structures of general time dependent dynamical systems," *Communications in Nonlinear Science and Numerical Simulation*, **18** (2013), 3530–3557.
- [38] A.J. Mariano, E.H. Ryan, H.S. Huntley, L.C Laurindo, E. Coelho, A. Griffa, ... and M. Wei, "Statistical properties of the surface velocity field in the northern Gulf of Mexico sampled by GLAD drifters," *Journal of Geophysical Research: Oceans*, **121** (2016), 5193–5216.
- [39] McWilliams, J. C, "Submesoscale currents in the ocean," *Proceedings of the Royal Society A: Mathematical, Physical and Engineering Sciences*, **472** (2016), 20160117.
- [40] P. Meunier, S. Le Dizes and T. Leweke, "Physics of vortex merging," *Comptes Rendus Physique*, **6** (2005), 431–450.
- [41] P. Miron, M.J. Olascoaga, F.J. Beron-Vera, N.F. Putman, J. Triñanes, R. Lumpkin and G.J. Goni, "Clustering of Marine Debris and Sargassum Like Drifters Explained by Inertial Particle Dynamics," *Geophysical Research Letters*, **47** (2020).
- [42] S. Mowlavi, M. Serra, E. Maiorino and L. Mahadevan, "Detecting Lagrangian coherent structures from sparse and noisy trajectory data," arXiv preprint (2021).
- [43] R. Mundel, E. Fredj, H. Gildor and V. Rom-Kedar, "New Lagrangian diagnostics for characterizing fluid flow mixing", *Phys. Fluids* **26**, 126602 (2014)
- [44] G. Novelli,C.M. Guigand, C. Cousin, E.H. Ryan, N.J. Laxague, H. Dai, B.K. Haus and T.M. Özgökmen, "A biodegradable surface drifter for ocean sampling on a massive scale," *Journal of Atmospheric and Oceanic Technology*, **34**(11) (2017), 2509–2532.
- [45] M.J. Olascoaga., F.J. Beron-Vera, G. Haller, J. Triñanes, M. Iskandarani, E. F. Coelho, B.K. Haus, H.S. Huntley, G. Jacobs, A.D. Kirwan and B.L. Lipphardt, "Drifter motion in the Gulf of Mexico constrained by altimetric Lagrangian coherent structures," *Geophysical Research Letters* **40** (2013): 6171–6175.
- [46] M.J. Olascoaga and G. Haller, Forecasting sudden changes in environmental pollution patterns. *Proceedings of the National Academy of Sciences*, **109** (2012), pp.4738-4743.
- [47] A. C. Poje, T.M. Özgökmen, B.L. Lipphardt, B.K. Haus, E.H. Ryan, A.C. Haza, ... and A. J. Mariano, "Submesoscale dispersion in the vicinity of the Deepwater Horizon spill," *Proceedings of the National Academy of Sciences*, **111**(35) (2014) , 12693-12698.
- [48] A. Provenzale, "Transport by coherent barotropic vortices," *Annual review of fluid mechanics*, **31**, pp.55–93.

- [49] P.L. Richardson, A.E. Strong and J.A. Knauss, "Gulf Stream eddies: Recent observations in the western Sargasso Sea. *Journal of Physical Oceanography*," **3** (1973), 297–301.
- [50] Richardson, P. L. (1993). A census of eddies observed in North Atlantic SOFAR float data. *Progress in Oceanography*, **31**(1), 1-50.
- [51] R. Rodríguez-Marroyo, A. Viúdez and S. Ruiz, "Vortex merger in oceanic tripoles," *Journal of Physical Oceanography*, **41** (2011), pp.1239–1251.
- [52] T. Rossby, M. Omand, J. Palter and D. Hebert, "On rates of isopycnal dispersion at the submesoscale," *Geophysical Research Letters*, **48** (2021).
- [53] A. Ruiz-Herrera, "Some examples related to the method of Lagrangian descriptors," *Chaos: An Interdisciplinary Journal of Nonlinear Science*, **25**(6) (2015), 063112.
- [54] A. Ruiz-Herrera, "Performance of Lagrangian descriptors and their variants in incompressible flows," *Chaos: An Interdisciplinary Journal of Nonlinear Science* **26**(10) (2016): 103116.
- [55] I.I. Rypina, S.E. Scott, L.J. Pratt and M.G. Brown, "Investigating the connection between complexity of isolated trajectories and Lagrangian coherent structures," *Nonlin. Proc. Geophys.* **18** (2011) 977–987.
- [56] B.L. Sawford, "Rotation of trajectories in Lagrangian stochastic models of turbulent dispersion," *Boundary-layer meteorology*, **93** (1999), pp.411–424.
- [57] K. L. Schlueter-Kuck and J.O. Dabiri, "Coherent structure colouring: identification of coherent structures from sparse data using graph theory," *Journal of Fluid Mechanics*, **811** (2017), 468-486.
- [58] T.G. Shepherd, J.N. Koshyk and K. Ngan, "On the nature of large-scale mixing in the stratosphere and mesosphere," *Journal of Geophysical Research: Atmospheres* **105**(D10) (2000): 12433-12446.
- [59] O.R. Southwick, E.R. Johnson and N.R. McDonald, "A simple model for sheddies: Ocean eddies formed from shed vorticity," *Journal of Physical Oceanography*, **46** (2016), pp.2961–2979.
- [60] O. R. Southwick, E.R. Johnson and N.R. McDonald, "Potential vorticity dynamics of coastal outflows," *Journal of Physical Oceanography*, **47** (2017), 1021–1041.
- [61] N. Tarshish, R. Abernathey, C. Zhang, C.O. Dufour, I. Frenger and S.M. Griffies, "Identifying Lagrangian coherent vortices in a mesoscale ocean model," *Ocean Modelling*, **130** (2018), pp.15–28.
- [62] E. van Sebille, M.H. England and G. Froyland, "Origin, dynamics and evolution of ocean garbage patches from observed surface drifters," *Environmental Research Letters*, **7** (2012).
- [63] M. Veneziani, A. Griffa, A.M. Reynolds and A.J. Mariano, "Oceanic turbulence and stochastic models from subsurface Lagrangian data for the Northwest Atlantic Ocean," *Journal of physical oceanography*, **34**(8) (2004), 1884-1906.
- [64] M. O. Williams, I.I. Rypina and C.W. Rowley, "Identifying finite-time coherent sets from limited quantities of Lagrangian data," *Chaos: An Interdisciplinary Journal of Nonlinear Science*, **25** (2015), 087408.